A Plasma Torus Around a Young Low-Mass Star

Luke G. Bouma[1,2]

[1] *Observatories of the Carnegie Institution for Science, Pasadena, CA 91101, USA*
[2] *Carnegie Fellow*

Approximately one percent of red dwarfs younger than 100 million years show structured, periodic optical light curves suggestive of transiting clumps of opaque material corotating with the star [1–4]. The composition, origin, and even the existence of this material are uncertain. The main alternative hypothesis is that these stars are explained by complex distributions of dark starspots or bright faculae distributed across their surfaces [5]. Here, we present time-series spectroscopy and photometry of a 40 million year old complex periodic variable (CPV), TIC 141146667. The spectra show coherent sinusoidal Balmer emission at up to four times the star's equatorial velocity, demonstrating the presence of extended clumps of circumstellar plasma — a plasma torus. Given that long-lived condensations of cool (10^4 K) plasma can persist in the hot (10^6 K) coronae of stars with a wide range of masses [6–11], these data support the idea that such condensations can become optically thick around the lowest-mass stars, although the exact source of opacity remains unclear.

1 Main

M dwarfs, stars with masses below about half that of the Sun, are the only type of star to offer near-term prospects for detecting the atmospheres of rocky exoplanets with water on their surfaces [12]. Investment with JWST has proceeded accordingly. How an M dwarf's evolution influences its planets—especially the retention of their atmospheres— has concurrently become a major theme in exoplanet and stellar astrophysics. Previous work has established that most M dwarfs host close-in planets [13] that are often subject to long circumstellar disk lifetimes [14], to large doses of UV radiation [15], and to a high incidence of flares and coronal mass ejections [16]. Nevertheless, despite excellent work in these areas, the properties of the circumstellar plasma and magnetospheric environments that bathe young, close-in exoplanets have remained challenging to quantify.

One glaring example of our current ignorance is the complex periodic variables (CPVs). Figure 1 highlights the main object of interest in this article, but over one hundred analogous objects have now been discovered by K2 and TESS [1–4,17,18]. These CPVs are defined by their highly structured and periodic optical light curves, and most are M dwarfs with rotation periods shorter than two days. Within current sensitivity limits, none have primordial disks [2,4]. However, $\approx$3% of stars a few million years old show this behavior, and the observed fraction decreases to $\approx$0.3% by $\approx$150 Myr [18].

The two leading hypotheses to explain the CPVs are either that transiting clumps of circumstellar material corotate with the star [2,4,19], or that these stars represent an extreme in naturally-occurring distributions of starspots or faculae [5]. Currently, the main argument against a starspot-

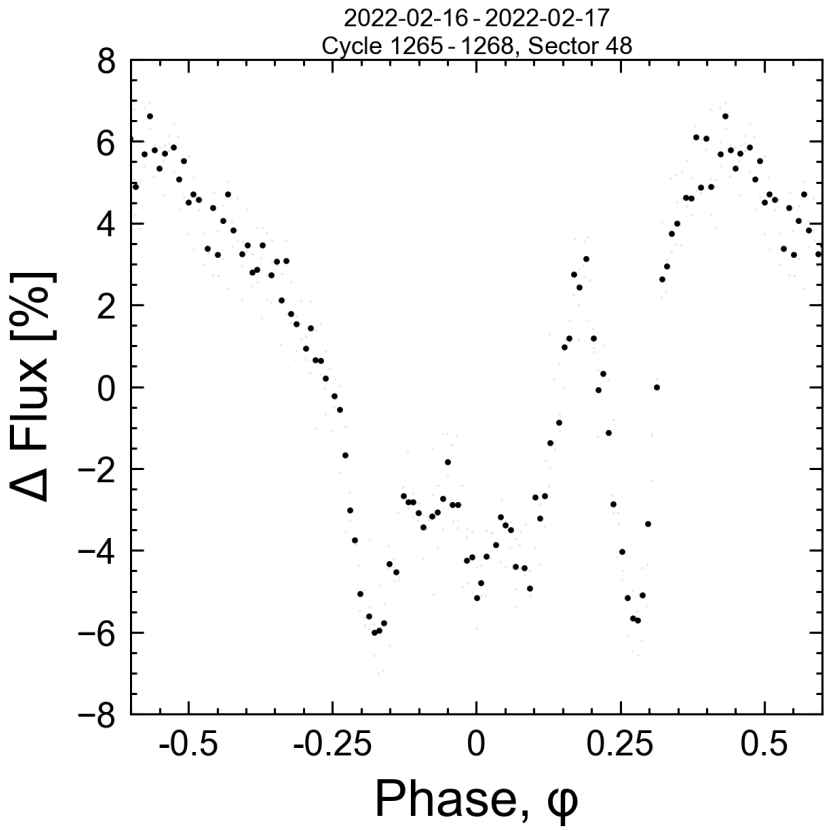

Figure 1: **Figure 1 (Movie): TIC 141146667 is a complex periodic variable (CPV).** For the best experience, please view the online movie available here, which spans a baseline of 5,784 cycles irregularly sampled over three years. The TESS light curve is phased to the 3.930 hour period in groups of a few cycles per frame. This is the period both of stellar rotation, and (we hypothesize) of corotating clumps of circumstellar material. Raw data acquired with two minute sampling are in gray; black is their average. Similar to other members of this class, the sharp photometric features persist for tens to thousands of rotational cycles.

only explanation invokes the timescales and amplitudes of the sharpest photometric features. However, no independent evidence has yet been acquired for the presence of circumstellar material in these objects. Since transiting circumstellar clumps would geometrically imply an intrinsic occurrence a few to ten times the observed rate, the question of whether circumstellar clumps exist in these systems has the potential to be applicable to 10-30% of M dwarfs during their early lives.

The dearth of evidence for circumstellar material around CPVs is surprising given that separate studies of young BAFGKM stars have, for decades, reported that stellar coronae contain both hot (10^6 K) and cool (10^4 K) plasma. In particular, time-series spectroscopy has shown periodic high-velocity absorption and emission in Balmer lines such as Hα, caused by long-lived, corotating

clumps of cool plasma [6,8,20,21]. Such clumps are forced into corotation by the magnetic field, and the exact geometry of where the plasma can accumulate is dictated by the magnetic field's topology. For instance, a tilted dipole field tends to yield an accumulation surface of a warped torus [7], whereas in the limit of a single strong field line, accumulation occurs along the apexpoint furthest from the star [10]. However, none of these spectroscopic variables have shown any photometric anomalies [4], leaving open the issue of whether these two areas of study have any direct connection. Nonetheless, CPVs do respond to sudden magnetic field changes: the otherwise long-lived eclipse features often disappear immediately following stellar flares [2,4].

In this study, we present the first observations of corotating clumps of cool plasma around a CPV. We identified TIC 141146667 in previous work [4] by searching the TESS two-minute data for stars showing periodic variability with at least three sharp dips per cycle. We selected the star for spectroscopic observations because its brightness and rapid rotation offered sensitivity to small variations in the line profiles. We observed it for five hours on UT 2024-02-17 using the High Resolution Echelle Spectrometer (HIRES; [22]) on the Keck I 10m telescope. TESS observed the star from UT 2024-02-05 to UT 2024-02-26 with a duty cycle of XX%. TESS was finishing a data downlink during the spectral observations, and photometric data collection resumed three rotation cycles (12 hours) after the spectra were acquired. Extended Data Figure 1 shows the detailed photometric behavior of the star before and after the exact epoch of observation; the star remained sufficiently stable to not affect the interpretation that follows.

2 Results

Figure 2 shows the data from February 2024. As expected based on other CPVs [4], the photometric shape of TIC 141146667 evolved following the 2022 discovery data, while nonetheless remaining complex. In February 2024, the average photometric signal showed a gradual brightening over 45% of the period, followed by a complex eclipse-like feature spanning 55% of the period. This eclipse feature shows two to three local photometric minima, and one to two local maxima. Its W-shape is suggestive of eclipse geometries seen in forward models of warped plasma tori [23].

The spectroscopy shows emission well beyond the star's equatorial velocity ($v_{\rm eq}$=130 $\rm km\,s^{-1}$). There are at least two distinct emission components, separated by half a cycle in phase. The first component has clearer sinusoidal behaviour and is double-peaked, with peak semi-amplitudes of K_1=2.1 $v_{\rm eq}$ and 2.7 $v_{\rm eq}$. There is significant non-periodic variability in this double-peaked component: the flux excess from both peaks begins with an amplitude equal to 100% of the continuum flux early in the observation sequence, and falls to 30% by its end. The component 180° opposite in phase is similarly only detected from ϕ=0.2-1.0. From ϕ=0.2-0.5, this latter component appears connected to the star in velocity space. While its peak semi-amplitude of K_1=3.9 $v_{\rm eq}$ is achieved at both ϕ=0.25 and 0.75, its amplitude decreases from a 60% excess over the continuum at the beginning of the observation sequence to a 10% excess by its end. The sinusoidal period for all of these emission components is consistent with the photometric 3.930 hour period.

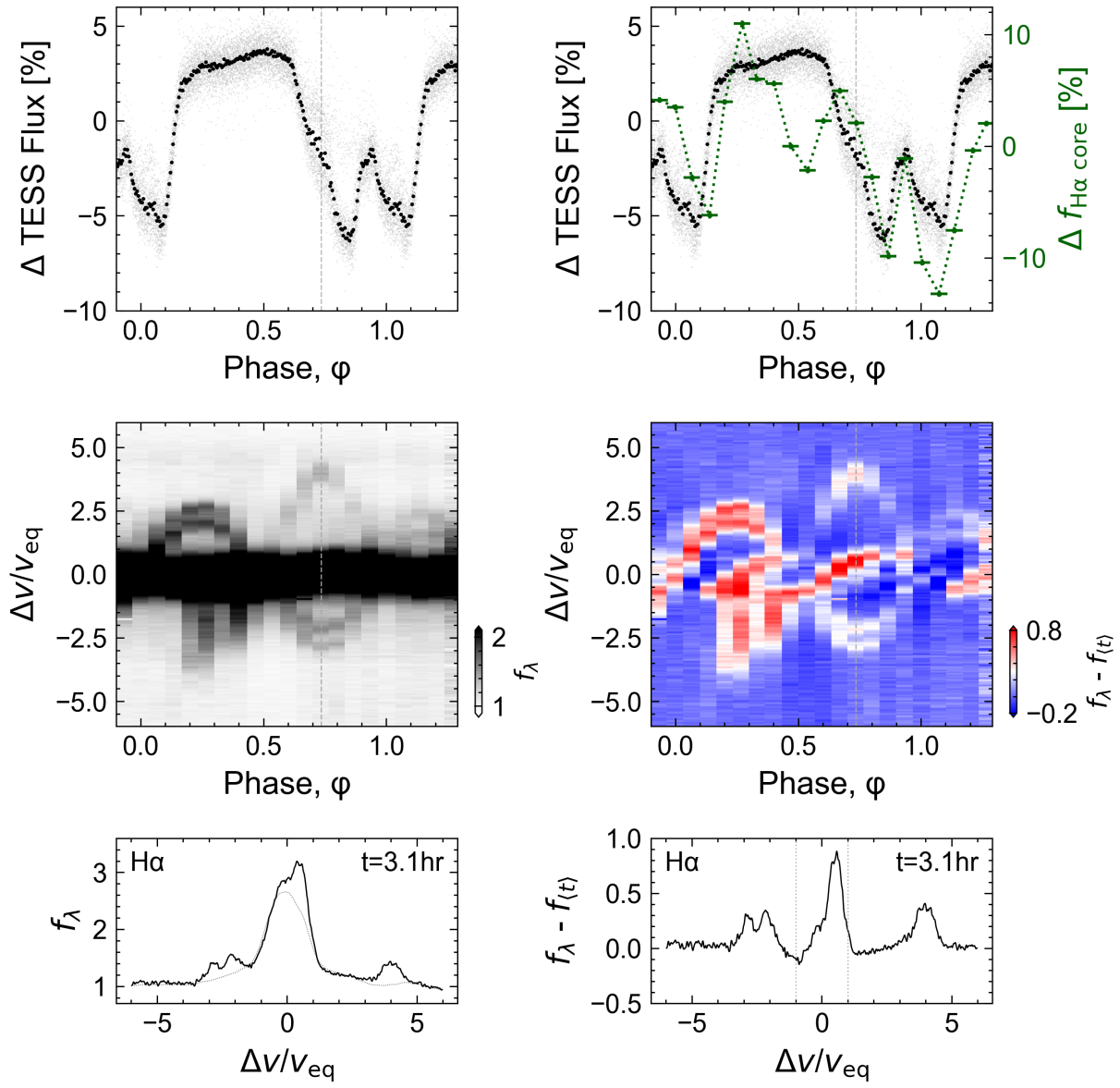

Figure 2: **Figure 2 (Movie):** Hydrogen emission from circumstellar plasma orbiting TIC 141146667. (**TODO**)For the best experience, please view the online movie available here. **Panel a:** TESS light curve from UT 2024-02-05 to UT 2024-02-26 folded on the 3.930 hour period. Black points are averaged; gray are the raw data. **Panel b:** Keck/HIRES Hα spectra acquired on UT 2024-02-17. The continuum is set to unity, and the darkest color is set at twice the continuum to accentuate emission outside the line core ($|v/v_{\rm eq}| > 1$, for $v_{\rm eq}$=130 km s^{-1}). While emission in the line core originates in the stellar chromosphere, the sinusoidal emission features are most readily described by a warped plasma torus. **Panel c:** Individual epochs of Panel b, visible in the online movie. The dotted line shows a time-averaged spectrum, $f_{\langle t \rangle}$. **Panel d:** As in Panel a, but overplotting the median-normalized Hα light curve at $|v/v_{\rm eq}| < 1$. **Panel e:** As in Panel b, after subtracting the time-averaged spectrum. In addition to circumstellar emission, the line core shows absorption during the plasma clump transits. The asymmetric stretch is set to match the dynamic range of the data. **Panel f:** Individual epochs of Panel e, visible in the online movie.

Table 1: Selected System Parameters for TIC 141146667

Parameter	Description	Value	Source
$T_{\rm eff}$	Effective Temperature (K)	2972 ± 40	1
$R_\star$	Stellar radius ($R_\odot$)	0.42±0.02	1
$M_\star$	Stellar mass ($M_\odot$)	XXX	6
γ	Systemic radial velocity ($\mathrm{km\,s^{-1}}$)	0.61 ± 1.47	1
Age	Adopted stellar age (Myr)	YYY	8
Spec. Type	Spectral Type	MXV	X
$P_{\rm rot}$	Rotation period (hr)	3.930 ± 0.001	X
$v_{\rm eq}$	Equatorial velocity ($2\pi R_\star/P_{\rm rot}$) ($\mathrm{km\,s^{-1}}$)	130±4	-
$v_{\rm eq} \sin i_\star$	Projected rotational velocity ($\mathrm{km\,s^{-1}}$)	128±3	X
$i_\star$	Stellar inclination (deg)	XXX	X
d	Distance (pc)	$57.6 \pm X.X$	X
$R_{\rm c}$	Keplerian corotation radius ($R_\star$)	XXX	X
a_1	Clump 1 orbital radius ($R_\star$)	2.1-2.7	X
a_2	Clump 2 orbital radius ($R_\star$)	3.9	X
$\langle \mathrm{EW_{H\alpha}} \rangle$	Time-averaged Hα line core equivalent width (Å)	X.X	Y
Range($\mathrm{EW_{H\alpha}}$)$_1$	Hα equiv. width range from Clump 1 (Å)	X.X	Y
Range($\mathrm{EW_{H\alpha}}$)$_2$	Hα equiv. width range from Clump 2 (Å)	X.X	Y

NOTE— is not resolved in the Gaia point source catalog. * Given only $v \sin i$ and $2\pi R_\star/P_{\rm rot}$, $\cos i = 0.11^{+0.11}_{-0.08}$. Provenances are: 1: SED fit[4], 2: TESS light curve,

These sinusoidal emission features require circumstellar clumps of partially-ionized hydrogen to be corotating with the star. The velocity semi-amplitude of the sinusoids gives the distance of these clumps from the stellar surface: 2.1-2.7 $R_\star$ for the closer clump, and 3.9 $R_\star$ for the other. This material's motion, rather than being Keplerian, can only be explained by plasma being dragged along with the rotating stellar magnetic field. These clumps transit in front of the star when passing from negative to positive velocity.

The behavior within the stellar Hα line core, at $|\Delta v/v_{\rm eq}| < 1$, is more complex than outside it. For stars of this age and spectral type, one would expect emission in the line core to be generated in the stellar chromosphere and then modulated by any occulting material capable of absorbing or emitting Hα photons. In Figure 2e, the behavior from ϕ=0.4-1.2 has a simple interpretation: from ϕ=0.4-0.9, a hot region first gradually crosses the stellar line profile, followed from ϕ=0.7-1.2 by the transit of a cool region. Phases ϕ<0.4 show a mix of similar events, though the time sampling is sufficiently coarse that the interpretation is less clear. A final exercise to quantify the behavior in the line core is shown in Figure 2d, where $f_{\rm H\alpha\ core}$ denotes the summed flux at $|\Delta v/v_{\rm eq}| < 1$. This panel shows that changes in the line core flux are usually correlated with the broadband variability, except at ϕ=0.5, during the transit of the higher-velocity clump and the occultation of the lower-velocity clump.

3 Discussion

Spectra of magetically-active, rapidly rotating stars with a wide range of masses have been known to exhibit both sinusoidal emission features [7,8,20,21] as well as sharp transient absorption features in their line cores [6,24,25] similar to those in Figure 2. No such stars were previously known to show complex light curves [4]. The usual interpretation for such variability comes from a loose analogy to quiescent solar prominences and filaments, which are cool condensations of plasma in the solar corona that can last days to weeks [26]. This plasma is called a prominence when viewed in emission against the dark backdrop of space, and a filament when viewed in absorption against the solar disk. In our Sun's magnetosphere, these condensations fall back to the solar surface because gravity is stronger than any magnetic or centrifugal force capable of sustaining them. However for stars with magnetospheric radii $R_{\rm m}$ that exceed their corotation radii $R_{\rm c}$, the effective potential experienced by a plasma parcel can have a local minimum outside $R_{\rm c}$, enabling the material to be sustained for much longer timescales [9,11]. Generally speaking, such material need neither transit, nor be optically thick.

Our Keck/HIRES observations are the first high-resolution time-series spectra of a CPV, and they show that corotating circumstellar plasma clumps are present in at least one such star. Characteristic densities and masses of these clumps are $n \sim 10^{10}\,{\rm cm}^{-3}$ and $M \sim 10^{14}\,{\rm kg}$ (see Supplementary Methods Section 3), a similar density to solar prominences, but ten to one hundred times more massive. This observation rules out a "starspot-only" origin scenario for CPVs, [5] since such scenarios have no means of explaining spectroscopic emission beyond the stellar disk. Similarly, scenarios in which the circumstellar material is made only of dust are also ruled out. While dust may be present, to explain the Hα emission the circumstellar clumps must include plasma with a significant population of hydrogen atoms in the n=3 excited state. While this plasma is undoubtedly sculpted by the star's magnetic field, it could plausibly originate from three sites: the star, an old and undetected disk, or outgassing rocky bodies. This latter possibility would render CPVs as extrasolar analogs of the Jupiter-Io plasma torus (CITE).

The other potential analog for the CPVs are the σ Ori E variables, a rare subset of B stars that with radiatively-driven winds that can accumulate into warped plasma tori [7,23]. These tori tend to have dense antipodal accumulations of plasma sculpted by tilted-dipole magnetic fields, and the transits of these clumps are thought to produce the observed broadband photometric variability through bound-free scattering [7] and Thomson scattering [27]. For σ Ori E and almost all of its analogs, the result is light curves that appear "simple", resembling those of eclipsing binaries [23]. The two known exceptions, HD 37776 and HD 64740, show complex light curves resembling CPVs [4,28] and have spectropolarimetric magnetic field maps indicating strong contributions from higher-order magnetic moments [29,30]. There are two implications: first, the complexity of CPVs may be a direct consequence of magnetic fields with highly multipolar contributions. Second, CPVs could be a source of astrophysical false positives in photometric searches for eclipsing binaries and transiting exoplanets around young pre-main-sequence M dwarfs [31,32].

Pressing issues for future work include determining the composition and origin of the circumstellar material, understanding the exact role of the stellar magnetic field, and exploring the implied space weather experienced by the close-in rocky exoplanets that, statistically [13], are likely to be present in most CPV systems.

The material's composition – either pure plasma, or else a dusty plasma – can be clarified by time-series optical and infrared spectrophotometry. While observations of CPVs in the optical have previously shown chromaticity consistent with dust [19,33,34], a gray opacity source such as electron scattering in a plasma transiting over starspots could also produce chromatic features [35]. The composition and size distribution of any dust that is present could be most easily resolved by measuring the extinction curve for one or more CPVs from 1-10 μm. A dust composition similar to debris from rocky bodies seen around white dwarfs [36] would indicate a rocky-body origin. A composition closer to the ISM would be indicative of condensed dust in an M dwarf wind, similar to that formed in the environments of more evolved stars [37].

The role of the star's magnetic field could be better understood through new observations, and new theory. From the theoretical perspective, there is an urgent need for rigid-field (magneto)-hydrodynamic modeling to go beyond previous work [7,23] and to explore the effects of non-dipolar field contributions. In particular, dynamo simulations of fully-convective M dwarfs have suggested the possibility that global-scale mean fields can be confined to a single hemisphere [38]; such fields would yield accumulations of circumstellar material quite different from those that have previously been explored [23]. Observationally, spectropolarimetry has the potential to assess both the field strength and topology. A more direct probe however might be to connected the recent work [39] showing that CPVs are variable radio emitters, exhibiting emission components that can be both persistent, as well as short-lived and highly polarized. This opens the prospects for detecting radio emission from the electron cyclotron maser instability, which would provide a direct measurement of the field strength at the site of the emitting region.

It is currently unclear what, if any, relationship CPVs have to the close-in exoplanets that exist around most M dwarfs [13]. However, 0.3-3% of young M dwarfs show the CPV phenomenon [18], and our data show that the phenomenon occurs when clumps of circumstellar material transit the star. The implied geometric correction suggests that an appreciable minority (3-30%) of M dwarfs – the rapidly rotating ones with centrifugal magnetospheres – have similar circumstellar environments to the CPVs.

Methods

Observations & Data Reduction *Photometry:* TESS observed TIC 141146667 (T=13.3) in Sectors 14, 15, 21, 41, 48, and 75. Two-minute data were acquired during Sectors 41, 48 (TESS DDT039, PI: Kunimoto), and 75 (TESS Program G06030, PI: Bouma). The data from Sectors 14, 15, and 21 had a 30-minute cadence, which smears sharp features over the $<$4 hour period (see [19]). The nearest known star, TIC 141146666 (T=14.5), is 25″ from TIC 141146667 and is photometrically stable in the pixel-level TESS data.

Figure 1 shows the data from Sector 75, which were acquired using the camera that points closest to the ecliptic. The largest gap in coverage is from BTJD 3356.0 - 3358.5, and includes the Keck/HIRES observation epoch (green bar). There are no flux measurements reported during this interval because the Earth was within 25° the camera's boresight, yielding high levels of

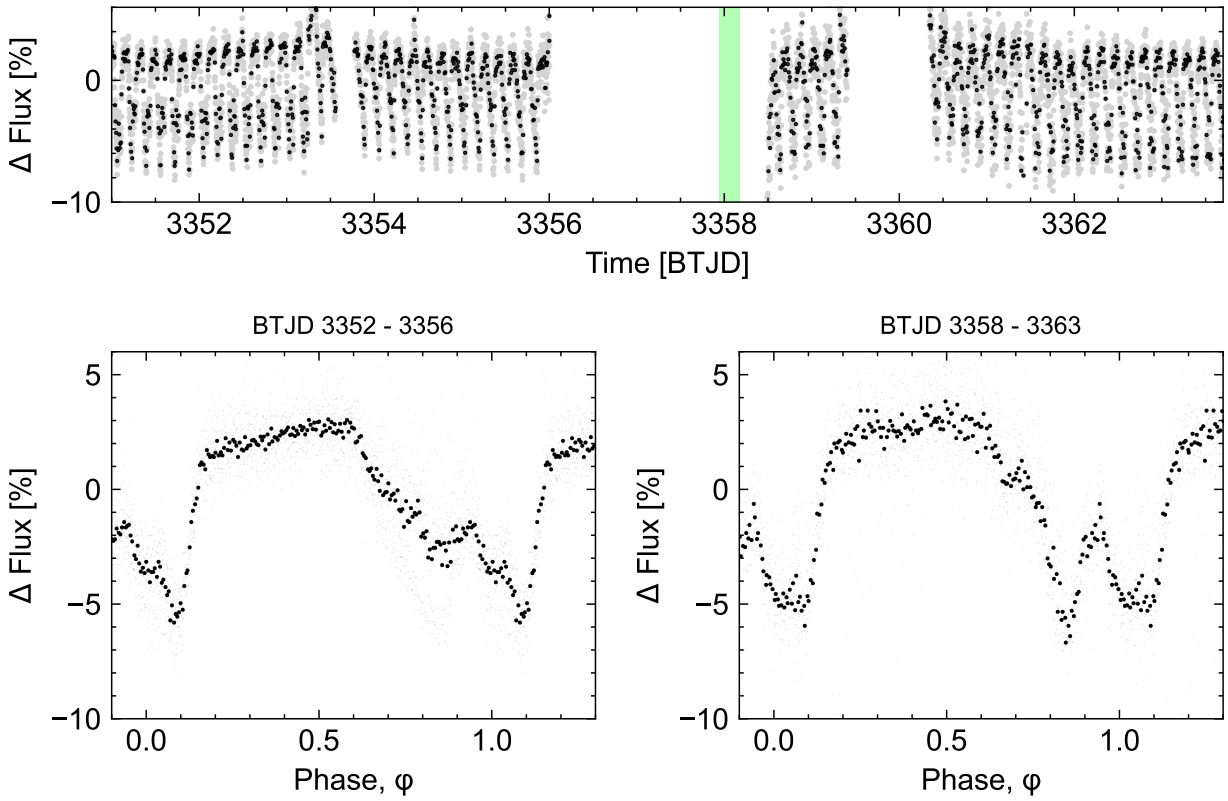

Extended Data Figure 1: Detailed photometric evolution of TIC 141146667 near the epoch of spectroscopic observation (green bar). **Panel a**: TESS simple aperture photometry acquired near time of Keck/HIRES observation. The main data gaps were caused by scattered light from the Earth and Moon, respectively. **Panels b,c**: Folded light curve before and after spectroscopy. While some evolution in the detailed light curve morphology occurred between the two epochs, the large, complex eclipse feature remained present.

scattered light. From BTJD 3359.4 - 3362.0, the Moon then passed within 25° of the camera's boresight. Based on the observed level of scattered light in the optimal TIC 141146667 aperture, we manually masked out times from 3359.4 - 3360.13, and judged the remainder of the data during the lunar approach to be usable. The small data gaps from BTJD 3353.55 - 3353.77 and from BTJD 3360.12 - 3360.33 were caused by data downlinks at the spacecraft's perigee and apogee, respectively.

Spectroscopy: We observed TIC 141146667 (V=16.2) with Keck/HIRES for five hours over a second-half night spanning UT 2024-02-17 10:47 to UT 2024-02-17 16:13. The star's airmass over this window spanned z=1.2-2.2, and we opted for a fixed 15 minute cadence over the entire sequence, except for a final 10 minute exposure due to increasing sky brightness at sunrise. We observed without the iodine cell and used the C2 decker ($0\farcs86\times14\farcs0$) in the red instrument configuration, yielding a spectral resolution R≈45,0000 (δv≈6.7 $\mathrm{km\,s^{-1}}$; $\delta v/v_{\rm eq}$≈0.05). We binned the CCD readout by a factor of three in the spatial dimension, yielding ≈1,000 photons (S/N=33) per pixel in the continuum at 6500 Å, at minimum airmass. Strong winds contributed to $1\farcs2\pm0\farcs2$ seeing over the night, but conditions were otherwise favorable. We reduced the echelleogram to a one-dimensional spectrum using the standard techniques of the California Planet Survey [40]. Figure 2 shows the result in the vicinity of Hα without any additional processing.

Spectroscopic Variability The full HIRES coverage spans 3650-7960 Å, and variable emission is visible in Balmer lines from n=10→2, Ca[H] and Ca[K], the Mg[I] b triplet, and the 5875 He[I] emission line.

Stellar Parameters *Radial Velocity*—We measured absolute radial velocities of TIC 141146667 from each of our spectra using a pipeline that we developed specifically for rapidly rotating stars. Our method is based on template-matching against synthetic spectra produced by the PHOENIX stellar atmosphere code [41]. We used the models with solar metallicity and alpha element abundances, and calibrated our absolute velocity zero-points as well as viable orders for velocity measurement using the standard stars described by [42]. We used velocity standards spanning spectral types from G2 to M4 (Barnard's Star), and included both slow and rapid rotators. We used `barycorrpy` [43] to calculate the velocity corrections due to Earth's motion around the solar system barycenter and due to Earth's daily rotation about its axis. Our analysis pipeline reproduces the systemic velocities reported by [42] for their velocity standards with an RMS of 0.66 $\mathrm{km\,s^{-1}}$.

For TIC 141146667, we measured the velocities from each of our HIRES spectra using regions near the K I (7700 Å) resonance line and three TiO bandheads (5160 Å, 5450 Å, and 5600 Å). These regions were selected and then averaged together because they provided the best matches between the synthetic and observed spectra, and therefore the most stable redshift measurements. The star's $130\pm4\,\mathrm{km\,s^{-1}}$ equatorial velocity and near-edge on viewing orientation yielded a line broadening $\Delta\lambda$≈3 Å. The scatter of resulting velocity measurements between each order to measure the RV precision at each epoch. The uncertainty-weighted mean velocity over all epochs on UT 2024-02-17 yields our adopted systemic radial velocity, $\gamma=0.6\pm1.5\,\mathrm{km\,s^{-1}}$. The relative radial velocities about this mean are given in Table 2. This radial velocity time-series rules out

any significant periodic change in velocities at the rotation period greater than 2.85 $\mathrm{km\,s^{-1}}$ (at 3σ confidence). This in turn sets an upper limit on the mass of any putative companions at this period of $m \sin i$<2.4 M_{Jup}.

Age: No Obvious Association Membership—Previous work [4] has shown that over 90% of CPVs are associated with known young moving groups based on their positions and kinematics. TIC 141146667 is one of the exceptions. We calculated the probability of TIC 141146667 being part of any of the nearby known groups using BANYAN Σ [?, v1.2;]Gagne2018, and based on that model, it appears to be a field star at >99.9% confidence. Searching the local vicinity of the star for neighbors with similar projected on-sky velocity [44] similarly yields no strong candidates for co-moving (Δv_{T}<5 $\mathrm{km\,s^{-1}}$) stars that share its isochronal youth.

Age: Isochrones— ∼TucHor or younger. Maybe 30-35myr? NB color puts it at M4.5 (main seq). BP-RP=3.3..

Age: Lithium— Frankly, it's not obviously there! (but maybe this is bc of the blending, and a pEW would show smth small)

Figure7 of Wood23 suggests from the Feiden Li depletion curves that no lithium would imply t¿37Myr. However Figure5 frmo the same work suggests maybe try binning up the spectrum, and then comparing against Bochanski+2007 for a lithium-free template.

Try differential comparison against Barnard's star...

This is weird. Are you 100% sure it's not a binary? Ups the need for the RV analysis.

Effective temperature, radius, and mass We adopt the results from the spectral energy distribution fitting exercise described by [4]. In brief, this approach used `astroARIADNE`... [45] with the BT-Settl stellar atmosphere models [46] assuming the [47] solar abundances, and the [48] water line lists. We used broadband magnitudes from Gaia DR2, APASS, 2MASS, SDSS, and WISE $W1$ and $W2$. (explain)...

Binarity

Spectral Behavior of Other Lines First, chromospheric:

Hγ, Hδ Line ratios.

Ca [K] Also shows some high-velocity emission. So, the emitting material has calcium ions.

He 5880 Also variable...

Magnesium b orders Shows some variability that is horrendously blended.

K[I] 7700 Literally the only obvious photospheric line.

Modeling the Emitting Clump The density and mass of the material...

1. Rebull, L. M. *et al.* Rotation in the Pleiades with K2. II. Multiperiod Stars. Astron. J. **152**, 114 (2016).

2. Stauffer, J. *et al.* Orbiting Clouds of Material at the Keplerian Co-rotation Radius of Rapidly Rotating Low-mass WTTs in Upper Sco. Astron. J. **153**, 152 (2017).

3. Rebull, L. M. *et al.* Rotation of Low-mass Stars in Upper Scorpius and ρ Ophiuchus with K2. Astron. J. **155**, 196 (2018).

4. Bouma, L. G. *et al.* Transient Corotating Clumps around Adolescent Low-mass Stars from Four Years of TESS. Astron. J. **167**, 38 (2024).

5. Koen, C. Starspot modelling of the TESS light curve of CVSO 30. Astron. Astrophys. **647**, L1 (2021).

6. Collier Cameron, A. & Robinson, R. D. Fast H-alpha variations on a rapidly rotating cool main sequence star- I. Circumstellar clouds. Mon. Not. R. Astron. Soc. **236**, 57–87 (1989).

7. Townsend, R. H. D. & Owocki, S. P. A rigidly rotating magnetosphere model for circumstellar emission from magnetic OB stars. Mon. Not. R. Astron. Soc. **357**, 251–264 (2005).

8. Dunstone, N. J., Collier Cameron, A., Barnes, J. R. & Jardine, M. The coronal structure of Speedy Mic - II. Prominence masses and off-disc emission. Mon. Not. R. Astron. Soc. **373**, 1308–1320 (2006).

9. Petit, V. *et al.* A magnetic confinement versus rotation classification of massive-star magnetospheres. Mon. Not. R. Astron. Soc. **429**, 398–422 (2013).

10. Waugh, R. F. P. & Jardine, M. M. Magnetic confinement of dense plasma inside (and outside) stellar coronae. Mon. Not. R. Astron. Soc. **514**, 5465–5477 (2022).

11. Daley-Yates, S. & Jardine, M. M. Simulating stellar coronal rain and slingshot prominences. Mon. Not. R. Astron. Soc. **534**, 621–633 (2024).

12. National Academies of Sciences, E. & Medicine. *Pathways to Discovery in Astronomy and Astrophysics for the 2020s* (The National Academies Press, Washington, DC, 2023). URL `https://nap.nationalacademies.org/catalog/26141/pathways-to-discovery-in-astronomy-and-astrophysics-for-the-2020s`.

13. Dressing, C. D. & Charbonneau, D. The Occurrence of Potentially Habitable Planets Orbiting M Dwarfs Estimated from the Full Kepler Dataset and an Empirical Measurement of the Detection Sensitivity. Astrophys. J. **807**, 45 (2015).

14. Ribas, Á., Bouy, H. & Merín, B. Protoplanetary disk lifetimes vs. stellar mass and possible implications for giant planet populations. Astron. Astrophys. **576**, A52 (2015).

Parameter	Host	Source
	Identifiers	
TIC	141146667	TESS
Gaia	860453786736413568	Gaia DR3
	Astrometry	
α	todo	Gaia DR3
δ	todo	Gaia DR3
μ_α (mas yr^{-1})	-73.933 $\pm$ 0.022	Gaia DR3
μ_δ (mas yr^{-1})	32.262 $\pm$ 0.024	Gaia DR3
π (mas)	17.324 $\pm$ 0.025	Gaia DR3
RUWE	1.23	Gaia DR3
	Photometry	
$TESS$ (mag)	todo	TESS
G (mag)	14.701 $\pm$ 0.002	Gaia DR3
$G_{\rm BP}$ (mag)	16.664 $\pm$ 0.008	Gaia DR3
$G_{\rm RP}$ (mag)	13.398 $\pm$ 0.006	Gaia DR3
$G_{\rm BP}$-$G_{\rm RP}$ (mag)	3.276 $\pm$ 0.010	Gaia DR3
J (mag)	11.401 $\pm$ 0.022	2MASS
H (mag)	10.793 $\pm$ 0.021	2MASS
K_s (mag)	10.473 $\pm$ 0.016	2MASS
$W1$ (mag)	10.276 $\pm$ 0.023	ALLWISE
$W2$ (mag)	10.070 $\pm$ 0.020	ALLWISE
$W3$ (mag)	9.838 $\pm$ 0.045	ALLWISE
	Kinematics and Position	
RV_{Bary} (km s^{-1})	13.35 ± 3.39	HIRES
U ($\mathrm{km\,s^{-1}}$)		
V ($\mathrm{km\,s^{-1}}$)		
W ($\mathrm{km\,s^{-1}}$)		
X (pc)	-28.4	
Y (pc)	19.8	
Z (pc)	67.0	
	Physical Properties	
P_{rot} (hours)	$3.930 \pm 0.XXX$	This work
$v \sin i_\star$(km s^{-1})	todo	This work
$i_\star$($^\circ$)	todo	This work
T_{eff} (K)	2972 $\pm$ 40	[4]
$R_\star$ ($R_\odot$)	0.42 $\pm$ 0.02	[4]
A_V (mag)	0	[49]
F_{bol} (erg cm^{-2} s^{-1})	todo	This work
$L_\star$ ($L_\odot$)	todo	This work
$M_\star$ ($M_\odot$)	todo	This work
$t_{\rm iso}$ (Myr)	16^{+19}_{-6}	This work

Extended Data Table 1: Properties of TIC 141146667.

Time [JD_{UTC}	RV ($\mathrm{km\,s^{-1}}$)	σ_{RV} ($\mathrm{km\,s^{-1}}$)
60357.450329	1.72	5.86
60357.461255	-5.41	2.37
60357.472181	-1.21	2.64
60357.483109	2.83	2.87
60357.494030	6.52	7.53
60357.504949	-3.0	1.44
60357.515873	0.01	1.21
60357.526794	-0.38	7.03
60357.537717	-3.92	2.71
60357.548639	7.92	6.75
60357.559566	4.94	8.84
60357.570487	-3.26	3.06
60357.581408	0.83	1.34
60357.592330	1.4	8.24
60357.603251	-8.05	3.94
60357.614172	-3.26	3.07
60357.625095	-3.84	7.55
60357.636019	-1.6	2.26
60357.646940	0.82	2.91
60357.657861	3.53	3.95
60357.668781	5.2	12.14

Extended Data Table 2: TIC 141146667 radial velocities.

15. France, K. *et al.* The Ultraviolet Radiation Environment around M dwarf Exoplanet Host Stars. Astrophys. J. **763**, 149 (2013).

16. Günther, M. N. *et al.* Stellar Flares from the First TESS Data Release: Exploring a New Sample of M Dwarfs. Astron. J. **159**, 60 (2020).

17. Zhan, Z. *et al.* Complex Rotational Modulation of Rapidly Rotating M Stars Observed with TESS. Astrophys. J. **876**, 127 (2019).

18. Rebull, L. M. *et al.* Rotation of Low-mass Stars in Taurus with K2. Astron. J. **159**, 273 (2020).

19. Günther, M. N. *et al.* Complex Modulation of Rapidly Rotating Young M Dwarfs: Adding Pieces to the Puzzle. Astron. J. **163**, 144 (2022).

20. Donati, J. F. *et al.* Surface differential rotation and prominences of the Lupus post T Tauri star RX J1508.6-4423. Mon. Not. R. Astron. Soc. **316**, 699–715 (2000).

21. Skelly, M. B. *et al.* Doppler images and chromospheric variability of TWA 6. Mon. Not. R. Astron. Soc. **385**, 708–718 (2008).

22. Vogt, S. S. *et al. SPIE Conference Series*, vol. 2198 (1994).

23. Townsend, R. H. D. Exploring the photometric signatures of magnetospheres around helium-strong stars. Mon. Not. R. Astron. Soc. **389**, 559–566 (2008).

24. Collier Cameron, A. & Woods, J. A. Prominence activity in G dwarfs of the alpha Persei cluster. Mon. Not. R. Astron. Soc. **258**, 360–370 (1992).

25. Cang, T. Q. *et al.* Magnetic field and prominences of the young, solar-like, ultra-rapid rotator V530 Persei. Astron. Astrophys. **643**, A39 (2020).

26. Vial, J.-C. & Engvold, O. *Solar Prominences*, vol. 415 of *Astrophysics and Space Science Library* (2015).

27. Berry, I. D., Owocki, S. P., Shultz, M. E. & ud-Doula, A. Electron scattering emission in the light curves of stars with centrifugal magnetospheres. Mon. Not. R. Astron. Soc. **511**, 4815–4825 (2022).

28. Mikulášek, Z. *et al.* What's New with Landstreet's Star HD 37776 (V901 Ori)? In Wade, G., Alecian, E., Bohlender, D. & Sigut, A. (eds.) *Stellar Magnetism: A Workshop in Honour of the Career and Contributions of John D. Landstreet*, vol. 11, 46–53 (2020). 1912.04121.

29. Kochukhov, O., Lundin, A., Romanyuk, I. & Kudryavtsev, D. The Extraordinary Complex Magnetic Field of the Helium-strong Star HD 37776. Astrophys. J. **726**, 24 (2011).

30. Shultz, M. E. *et al.* The magnetic early B-type stars I: magnetometry and rotation. Mon. Not. R. Astron. Soc. **475**, 5144–5178 (2018).

31. Johns-Krull, C. M. *et al.* Hα Variability in PTFO8-8695 and the Possible Direct Detection of Emission from a 2 Million Year Old Evaporating Hot Jupiter. Astrophys. J. **830**, 15 (2016).

32. Bouma, L. G. *et al.* PTFO 8-8695: Two Stars, Two Signals, No Planet. Astron. J. **160**, 86 (2020).

33. Tanimoto, Y. *et al.* Evidence for planetary hypothesis for PTFO 8-8695 b with five-year optical/infrared monitoring observations. PASJ **72**, 23 (2020).

34. Koen, C. Multifilter observations of the complex periodic variations in eight pre-main sequence stars. Mon. Not. R. Astron. Soc. **518**, 2921–2937 (2023).

35. Rackham, B. V., Apai, D. & Giampapa, M. S. The Transit Light Source Effect: False Spectral Features and Incorrect Densities for M-dwarf Transiting Planets. Astrophys. J. **853**, 122 (2018).

36. Reach, W. T., Lisse, C., von Hippel, T. & Mullally, F. The Dust Cloud around the White Dwarf G 29-38. II. Spectrum from 5 to 40 μm and Mid-Infrared Photometric Variability. Astrophys. J. **693**, 697–712 (2009).

37. Marigo, P. *et al.* Evolution of asymptotic giant branch stars. II. Optical to far-infrared isochrones with improved TP-AGB models. Astron. Astrophys. **482**, 883–905 (2008).

38. Brown, B. P., Oishi, J. S., Vasil, G. M., Lecoanet, D. & Burns, K. J. Single-hemisphere Dynamos in M-dwarf Stars. Astrophys. J. **902**, L3 (2020).

39. Kaur, S. *et al.* Hints of auroral and magnetospheric polarized radio emission from the scallop-shell star 2MASS J05082729–2101444. Astron. Astrophys. **691**, L17 (2024).

40. Howard, A. W. *et al.* The California Planet Survey. I. Four New Giant Exoplanets. Astrophys. J. **721**, 1467–1481 (2010).

41. Husser, T. O. *et al.* A new extensive library of PHOENIX stellar atmospheres and synthetic spectra. Astron. Astrophys. **553**, A6 (2013).

42. Chubak, C. *et al.* Precise Radial Velocities of 2046 Nearby FGKM Stars and 131 Standards. *arXiv e-prints* arXiv:1207.6212 (2012).

43. Kanodia, S. & Wright, J. Python Leap Second Management and Implementation of Precise Barycentric Correction (barycorrpy). *Research Notes of the American Astronomical Society* **2**, 4 (2018).

44. Tofflemire, B. M. *et al.* TESS Hunt for Young and Maturing Exoplanets (THYME). V. A Sub-Neptune Transiting a Young Star in a Newly Discovered 250 Myr Association. Astron. J. **161**, 171 (2021).

45. Vines, J. I. & Jenkins, J. S. ARIADNE: measuring accurate and precise stellar parameters through SED fitting. Mon. Not. R. Astron. Soc. **513**, 2719–2731 (2022).

46. Allard, F., Homeier, D. & Freytag, B. Models of very-low-mass stars, brown dwarfs and exoplanets. *Philosophical Transactions of the Royal Society A: Mathematical, Physical and Engineering Sciences* **370**, 2765–2777 (2012).

47. Asplund, M., Grevesse, N., Sauval, A. J. & Scott, P. The Chemical Composition of the Sun. ARA&A **47**, 481–522 (2009).

48. Barber, R. J., Tennyson, J., Harris, G. J. & Tolchenov, R. N. A high-accuracy computed water line list. Mon. Not. R. Astron. Soc. **368**, 1087–1094 (2006).

49. Green, G. M., Schlafly, E., Zucker, C., Speagle, J. S. & Finkbeiner, D. A 3D Dust Map Based on Gaia, Pan-STARRS 1, and 2MASS. Astrophys. J. **887**, 93 (2019).

Acknowledgments The author thanks X, Y, Z. L.G.B. was suported by... Acknowledge TESS...

Author Contributions ...

Data Availability ...

Competing Interests The authors declare that they have no competing financial interests.

Correspondence Correspondence and requests for materials should be addressed to ...

Code availability We provide access to a GitHub repository including all code created for the analysis of this project that is not already publicly available.